Zhou *et al. Advances in Aerodynamics* (2023) 5:26
https://doi.org/10.1186/s42774-023-00158-w

Advances in Aerodynamics

RESEARCH Open Access

Effects of non-stationary wind velocity models on buffeting performance of closed-box girder suspension bridges

Rui Zhou[1], Yinan Lin[1], Peng Lu[1], Yongxin Yang[2*] and Jinbo Zhu[2]

*Correspondence:
yang_y_x@tongji.edu.cn

[1] College of Civil and Transportation Engineering, Shenzhen University, Shenzhen 518060, China
[2] State Key Laboratory for Disaster Reduction in Civil Engineering, Tongji University, Shanghai 200092, China

Abstract

Non-stationary characteristic in nature wind has a great effect on buffeting performance of long-span bridges. The influence of key parameters in non-stationary wind velocity models on nonlinear buffeting responses of a super long-span suspension bridge was investigated in this paper. Firstly, four non-stationary wind velocity models are established by combing the time-varying average wind velocity with an exponential function and the fluctuating wind velocity with four modulation functions, respectively. These non-stationary wind velocity models have obvious non-stationary characteristics and then are validated by the classical power spectrum densities. Finally, three displacement responses of the bridge deck under four different independent variables of β in the exponential function and four modulation functions were compared, respectively. Results show that the turbulence intensities using two non-uniform modulation functions (NMF) are larger than those using uniform modulation functions (uMF). Moreover, the root mean square (RMS) values of three displacement responses increase with the decrease of β. Besides, the RMS values of three displacement under two NMFs are larger than those under two uMFs, and their RMS values under the second uMF are the smallest.

Keywords: Suspension bridge, Time-varying average wind velocity, Uniform modulation function, Non-uniform modulation function, Non-stationary wind velocity, Buffeting displacement response

1 Introduction

With the rapid development of long-span bridge technology, more and more super long-span suspension bridges with closed-box girders have been designed and constructed overall the world, for example, the 1915 Canakkale Bridge in Turkey with a main span of 2023 m was in operation in February 2022. Compared with the twin-box girder [1], the closed-box girder suspension bridge is more susceptible to wind loads owing to its low stiffness, and its limit span without countermeasures is regarded as about 1500 m [2, 3]. Meanwhile, strong typhoons have frequently occurred in China in recent years, such as the strong typhoon Lekima in 2019 with 16-level landfall in Zhejiang Province, China. As a prominent characteristic of strong typhoons, the non-stationary wind velocity has

a significant impact on buffeting performance of super long-span suspension bridges, which could lead to discomfort for passengers and structural fatigue damage to bridges [4–6]. In order to accurately predict the buffeting performance under strong typhoons, it is essential to investigate the effect of critical parameters of non-stationary wind velocity on the buffeting responses of super long-span suspension bridges with closed-box girders.

In the wind field analysis, non-stationary wind velocity is usually composed of the average wind velocity and the fluctuating wind velocity [7]. On one hand, many researchers have studied the time-varying characteristics of the average wind velocity of typhoons at the bridge location based on the typhoon field measurement. Xu et al. [8] analyzed the time-varying average wind velocity from Typhoon Victor at the bridge site of the Tsing Ma suspension Bridge by applying the empirical mode decomposition. Hu et al. [9] adopted the wavelet transform method to obtain the time-varying average wind velocity, and proposed an effective wavelet-based nonstationary wind velocity model. Zhao et al. [10] studied the wind characteristics over water terrain when the outer regions of four typhoons passed the bridge. On the other hand, the time-varying average wind velocity of a typhoon is assumed to be a special function. Liu et al. [11, 12] applied the cubic spline function to simulate the time-varying average wind velocity of the hurricane and derived the non-uniform modulation function of the evolutionary power spectrum. Bao et al. [13] presented a new method of time–frequency interpolation to conduct two rounds of spline interpolation, which could agree well with the target spectra. Tubino et al. [14] compared the effects of various weighted functions on the harmonic content and statistical properties of turbulence. In the absence of measured wind velocity data, the average wind velocity is generally assumed to be a time-varying exponential function [15], while the role of a key coefficient in the exponential function of the average wind velocity should be further identified.

As for Priestley's evolutionary spectral theory in the fluctuating wind velocity model of non-stationary wind, Hu et al. [16] proposed a non-stationary typhoon model in complex terrain to predict the non-stationary buffeting performance of bridges. Li et al. [17] proposed a spectral-representation-based method to extract the inseparable time and frequency components of the evolutionary power spectral density function using Taylor series expansion. Tao et al. [18, 19] evaluated the non-stationary buffeting performance of the Stonecutters Bridge due to the time-varying fluctuating wind coherence of Typhoon Hato. Huang et al. [20] established a conditional simulation approach to establish the multi-variable non-stationary typhoon wind for bridges, which takes into account a non-modulation function of the fluctuating wind. Su et al. [4] presented an efficient frequency domain scheme based on fast complete quadratic combination (CQC) method, which was applied to evaluate the buffeting response of a long-span suspension bridge located in a complex mountainous wind environment. However, the effects of different uniform and non-uniform modulation functions of fluctuating wind velocity models on the buffeting performance of super long-span suspension bridges are unclear.

In order to accurately predict the buffeting performance of super long-span suspension bridges under the non-stationary wind, the nonlinear buffeting responses of a suspension bridge with a main span of 580 + 1756 + 630 m under four typical non-stationary wind

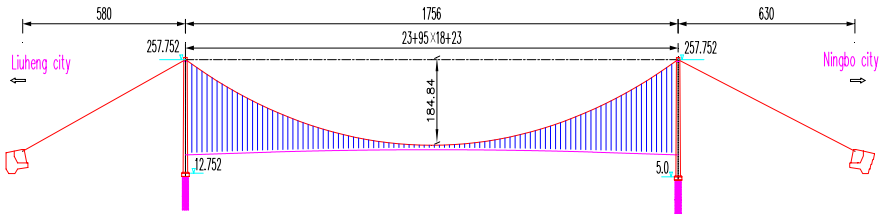

Fig. 1 Structural layout of the suspension bridge (Unit: m)

Table 1 Structural parameters of the bridge with a closed-box girder

Width B / m	Height H / m	Mass per unit length M / kg/m	Mass moment of inertia I_m/ kg·m^2/m	Vertical frequency f_h / Hz	Torsional frequency f_t / Hz
41.7	3.5	3.27e^4	5.69e^6	0.0895	0.221

velocity models are analyzed in this paper. Firstly, the time-varying average wind velocity with an exponential function and the fluctuating wind velocity with two common uniform and two non-uniform modulation functions are selected to establish four non-stationary wind models, which were then validated by classical spectra. Based on the nonlinear finite element model of the 3D bridge combined with the nonlinear buffeting force model of a 2D closed-box girder, the maximum displacement responses along the bridge deck were compared by an exponential function with four different coefficient values (i.e. β = 1000, 1500, 2000, 2500). Finally, buffeting displacement responses of the bridge deck were further investigated under four non-stationary wind velocity models with different modulation functions, respectively. This present study is helpful to effectively evaluate the wind-resistance performance of suspension bridges under specific wind events.

2 Non-stationary wind models

2.1 Wind parameters at the bridge site

A super long-span suspension bridge with three spans of 580 + 1756 + 630 m was chosen as a typical bridge project, which was designed in the Ningbo City of Zhejiang province, China. As shown in Fig. 1, the heights of two side towers are 245 m and 252.752 m with reinforced concrete structures, and the stage-to-span ratio of the cable is 1/9.5 with a longitudinal distance of 18 m between two adjacent suspenders. The structure parameters of the suspension bridge are presented in Table 1.

Based on the Wind-resistant Design Specification (JTG/T 3360-01-2018) for Highway Bridges in China, the associated average wind velocity at the bridge site is considered to be $\overline{U}_{\text{ref}}$ = 44.3 m/s at the reference height of Z_{ref} = 10 m. Furthermore, as the B-type terrain [21], z_0 = 0.01 and α = 0.12 in the wind field simulation at the bridge site. Therefore, the reference average wind velocity at the height of the main span with z_i = 70 m is $\overline{U}_{\text{ref},i} = \overline{U}_{\text{ref}}(\frac{z_i}{z_{\text{ref}}})^{\alpha} = 44.3 \times (\frac{70}{10})^{0.14} = 58.7$ m/s.

2.2 Four non-stationary wind velocity models

The non-stationary wind velocity is the sum of the time-varying average velocity and the fluctuating wind velocity. The time-varying mean wind in the non-stationary wind model could be assumed to be a special function, and the cosine function is a common special function [22], as described in Eq. (1):

$$\overline{U} = \overline{U}_{\mathrm{ref},i}\exp(t/\beta). \tag{1}$$

Where $\overline{U}$ is the time-varying average wind velocity at the bridge deck, β is the independent variable of the exponential function, and t is the time.

Based on Priestley's evolutionary spectral theory [15], the uniform and non-uniform modulation functions are often used to modulate the classical power spectrums, in which two typical uniform modulation functions (namely, uMF1 and uMF2) and two typical non-uniform modulation functions (namely, NMF1 and NMF2) are selected to simulate the fluctuating wind velocities in this paper. The expression of the first uniform modulation function [17–19] in uMF1 is Eq. (2):

$$A(t) = \exp(-(t-\alpha)^2/\delta). \tag{2}$$

Where α and δ are the feature parameters of Eq. (2), which are defined as 200 and 18,000 in the assumption of time-varying wind spectra of Typhoon Hato, respectively.

The expression of the second uniform modulation function [23] in uMF2 is Eq. (3):

$$A(t) = \frac{e^{-0.1t} - e^{-0.2t}}{0.25}. \tag{3}$$

The expression of the first non-uniform modulation function [22] in NMF1 is Eq. (4):

$$G(\omega,t) = A^2(\omega,t)S(\omega,t), A(\omega,t) = \sqrt{\frac{\overline{U}}{U(t)}\frac{\left[1+50\frac{\omega z}{2\pi\overline{U}}\right]^{5/3}}{\left[1+50\frac{\omega z}{2\pi U(t)}\right]^{5/3}}}. \tag{4}$$

Where $G(\omega,t)$ is the evolutionary spectral and $A(\omega,t)$ is the non-uniform modulation function, z is the bridge deck's height, and ω is the frequency.

The express of the second non-uniform modulation function [20] in NMF2 is the Eq. (5):

$$S(\omega,t) = A^2(\omega,t)\frac{1066.67}{\left[1+70.8(50\omega/3)^2\right]^{5/6}}, A(\omega,t) = 0.5\exp\left[-0.001(t-500)^2\omega^{0.9}\right]+0.5. \tag{5}$$

The multi-variable random wind field at the bridge site with the combination of the time-varying average wind velocity and the fluctuating wind velocity is obtained by using the Weighted Amplitude Wave Superposition method and the Inverse Fast Fourier Transform (FFT) method [7, 24]. Twenty-eight points along the bridge deck are used to generate the wind field with an interval of 62.7 m. The time step and total time of the wind field simulation are 0.1 s and 900 s, respectively. The total frequency component is 1024 and the sample frequency number is 256. As the examples of $\beta = 2500$ in Eq. (1),

the time histories of vertical and along-wind wind velocities at the mid-span of four non-stationary wind velocity models are illustrated in Fig. 2, respectively.

Under the four non-stationary wind velocity models, the simulated vertical wind velocity always fluctuates around zero, and thus the vertical wind velocity has an obvious time-varying variance. The horizontal (along-wind) wind velocity is the sum of the average wind velocity and the fluctuating wind velocity, and presents an upward trend with the increase of time and fluctuates in different periods, which reflect the time-varying variance and frequency of the non-stationary wind velocity. Therefore, the fluctuation ranges of wind velocity in the horizontal direction are much larger than those in the vertical direction, and all of these simulated wind velocity models have obvious non-stationary characteristics.

2.3 Validation of wind velocity models

As listed in Table 2, the turbulence intensities I_u of these non-stationary wind velocity models (i.e., two examples of uMF1 and NMF1) are tested in the vertical and horizontal turbulence, respectively. All of the simulated vertical turbulence intensities are smaller than those of the target values, but their errors are still smaller than 30%. The simulated horizontal turbulence intensities of the uMF1 are much smaller than those of the target values, while the simulated horizontal turbulence intensities of the

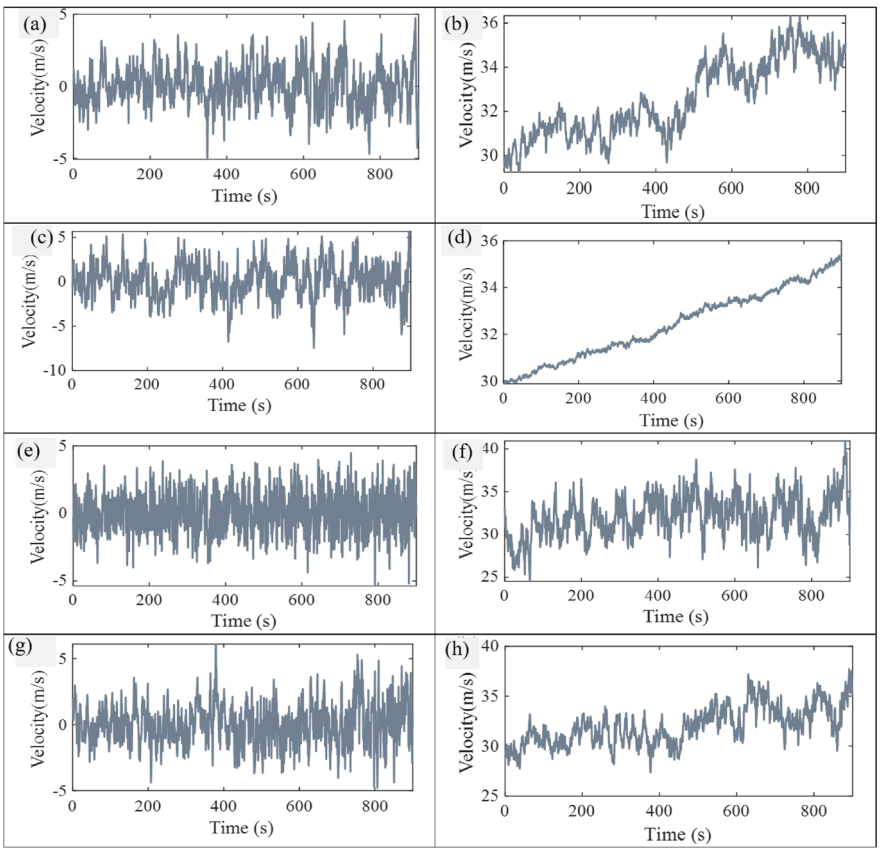

Fig. 2 Vertical and horizontal non-stationary wind velocities at the midspan: **a**-**b** time histories under uMF1; **c**-**d** time histories under uMF2; **e**-**f** time histories under NMF1; **g**-**h** time histories under NMF2

Table2 Turbulence intensity I_u testing of non-stationary wind velocity models

	I_u	uMF1			NMF1		
		1/2L	1/4L	3/4L	1/2L	1/4L	3/4L
Vertical turbulence	Simulation (%)	0.054	0.052	0.054	0.069	0.069	0.070
	Target (%)	0.070	0.070	0.070	0.070	0.070	0.070
	Error (%)	22.9	25.7	22.9	1.4	1.4	0
Horizontal turbulence	Simulation (%)	0.093	0.095	0.095	0.149	0.156	0.150
	Target (%)	0.130	0.130	0.130	0.130	0.130	0.130
	Error (%)	28.5	26.9	26.9	14.6	20.0	15.4

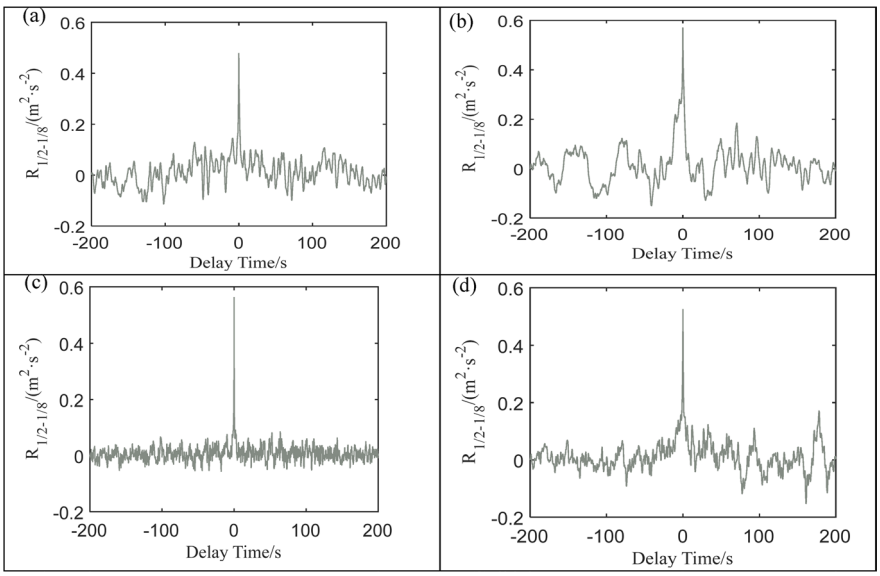

Fig. 3 Comparison between the vertical wind velocity correlation between the 1/2L and 1/8L of the bridge deck: **a** uMF1; **b** uMF2; **c** NMF1; **d** NMF2

NMF1 are larger than those of the target values. Meanwhile, the simulated turbulence intensities at 1/2L are close to those at 1/4L or 3/4L. As a consequence, the turbulence intensities by using non-uniform modulation functions are larger than those by using uniform modulation functions.

Figures 3 and 4 describe the vertical and horizontal cross-correlation of the fluctuating wind velocity at the 1/2L and 1/8L under the four non-stationary wind velocity models, respectively. The cross-correlation coefficients of the vertical wind velocity decrease rapidly from the maximum value at zero time to the low value at other times, while the cross-correlation coefficients of the horizontal wind velocity slowly decrease, which indicates that the non-stationarity of the horizontal fluctuating wind velocity is stronger. Furthermore, the cross-correlation coefficients of the simulated horizontal wind velocity are larger than those of the vertical wind velocity, and the spatial correlation of the simulated horizontal fluctuating wind velocity is also stronger.

The Panofsky power spectrum and the Kaimal power spectrum are selected to represent the classic vertical and along-wind horizontal fluctuating wind spectra [25, 26]. Where S_u and S_w are auto-spectral density functions in the horizontal and vertical

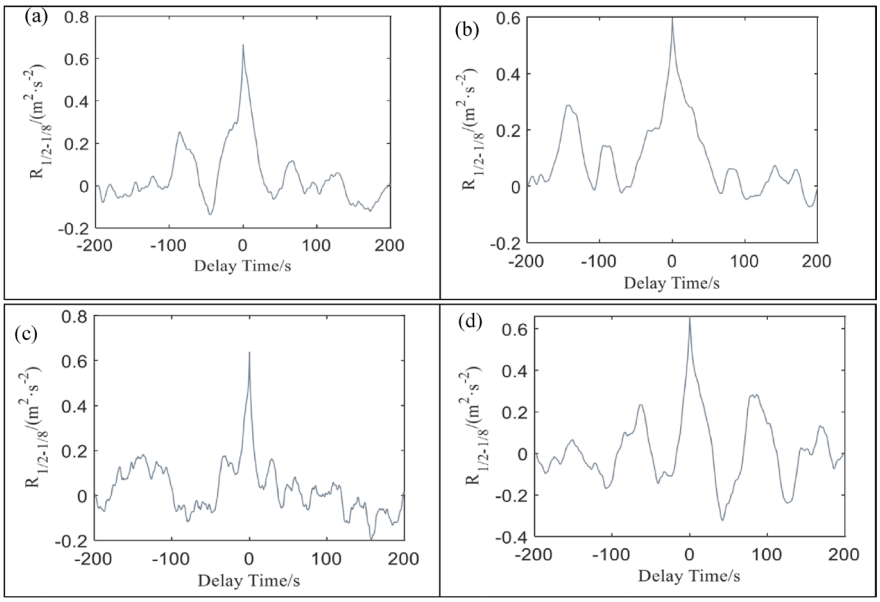

Fig. 4 Comparison between the horizontal wind velocity correlation between the 1/2L and 1/8L of the bridge deck: **a** uMF1; **b** uMF2; **c** NMF1; **d** NMF2

directions, n is the natural frequency of the fluctuating wind, u is the wind velocity, and f is the non-dimensional normalized frequency.

$$\text{Karmal power spectrum}: \frac{nS_u(n)}{u_*^2} = \frac{200f}{(1+50f)^{5/3}}. \tag{6}$$

$$\text{Panofsky power spectrum}: \frac{nS_w(n)}{u_*^2} = \frac{6f}{(1+4f)^2}. \tag{7}$$

The simulated power spectrum density (PSD) of five wind velocity models without and with the evolution spectrum are compared with the corresponding classical wind spectra, as plotted in Fig. 5. Under four non-stationary wind velocity models, the high-frequency parts of the simulated PSD are close to the classical power spectrums, and the low-frequency parts of the simulated PSD are slightly higher than those of the classical power spectra. As two examples of uMF1 and NMF1, these non-stationary wind velocity models could effectively simulate the non-stationary characteristics, regardless of the horizontal and vertical wind velocity.

3 Buffeting responses under four non-stationary wind velocity models

3.1 Nonlinear finite element model of the bridge

Based on the developed nonlinear buffeting force model (NBFM), the detailed parameters of the NBFM for the closed-box girder are identified, including the coefficients of static aerodynamic force, self-excited force, and the buffeting force [7, 24]. Figure 6 displays a three-dimensional nonlinear finite element bridge

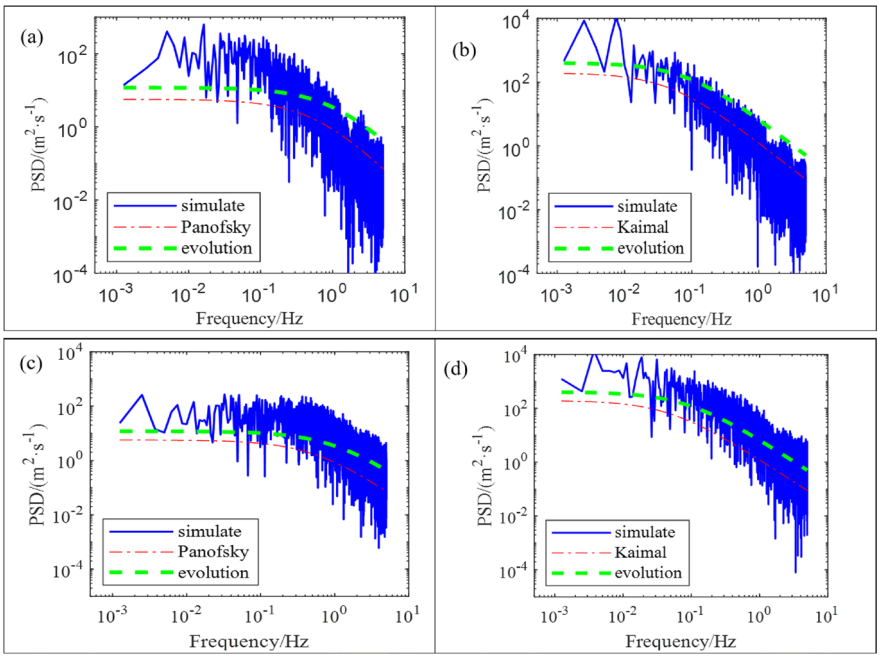

Fig. 5 Comparison among the simulated PSD, the classical PSD, and the evolutionary PSD: **a**-**b** vertical and horizontal PSD under uMF1; **c**-**d** vertical and horizontal PSD under NMF1

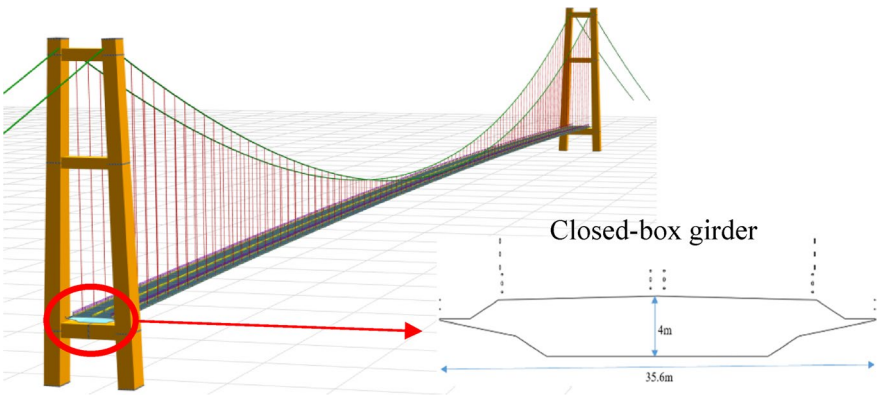

Fig. 6 Nonlinear finite element model of the bridge with the closed-box girder

model integrated with the NBFM of the 2D closed-box girder which is simulated by the nonlinear aerodynamic force elements with 6 nodal degrees of freedom and a set of self-excited force and buffeting force subsystem degrees of freedom. The 3D beam element is used to simulate the closed-box girder and main towers, and the 3D truss element is used to simulate the main cables and hanger with the total elements of 881. Their nonlinear buffeting displacement responses are solved by the combination of the Newton–Raphson method and the Newmark-β method under the above four non-stationary wind velocity models.

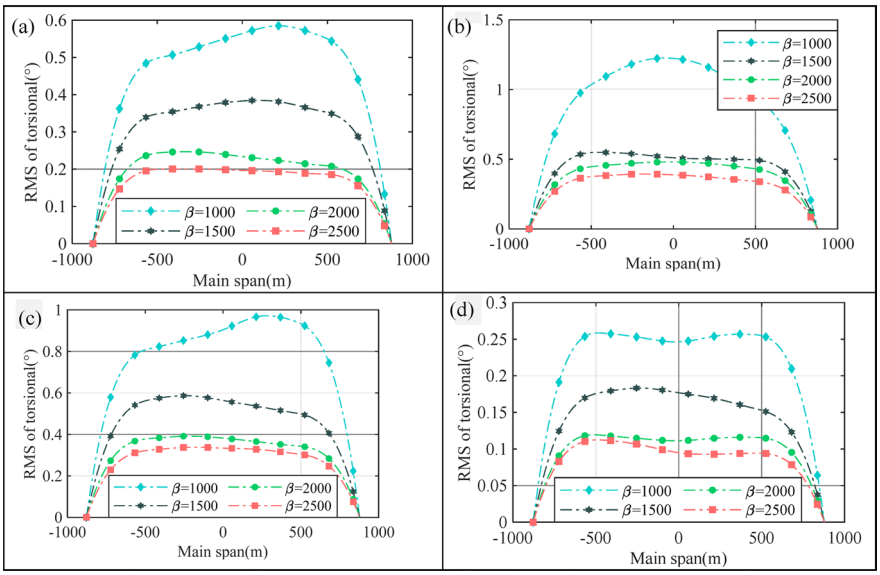

Fig. 7 Torsional displacement comparison of the bridge deck: **a** uMF1; **b** uMF2; **c** NMF1; **d** NMF2

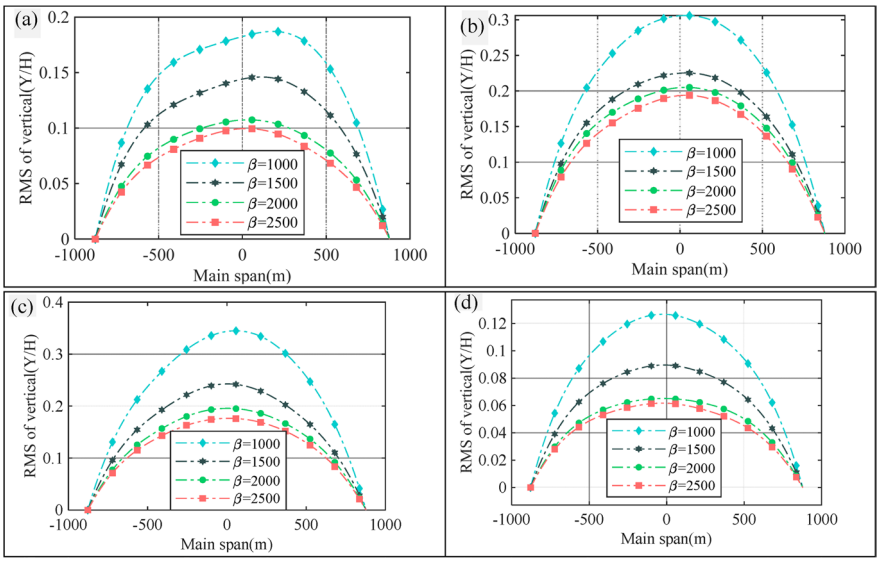

Fig. 8 Vertical displacement comparison of the bridge deck: **a** uMF1; **b** uMF2; **c** NMF1; **d** NMF2

3.2 Buffeting responses under various time-varying average wind velocities

Since the key factor β is related to the amplitude of average wind velocity in non-stationary typhoons, four typical different values of the β (e.g., $\beta = 1000$, 1500, 2000, and 2500) are used to investigate the effect of time-varying average wind velocity on the nonlinear buffeting responses of the bridge. The RMS (root mean square) values of three displacement responses along the whole bridge deck under four values of β are compared in Figs. 7, 8 and 9, respectively. With the increase of the β, all the RMS values of three displacement responses significantly become smaller, especially when the β changes from 2000 to 1500. As for the torsional displacement responses at the 1/2L, the RMS values of torsional displacement under the uMF2 are the largest, while the RMS

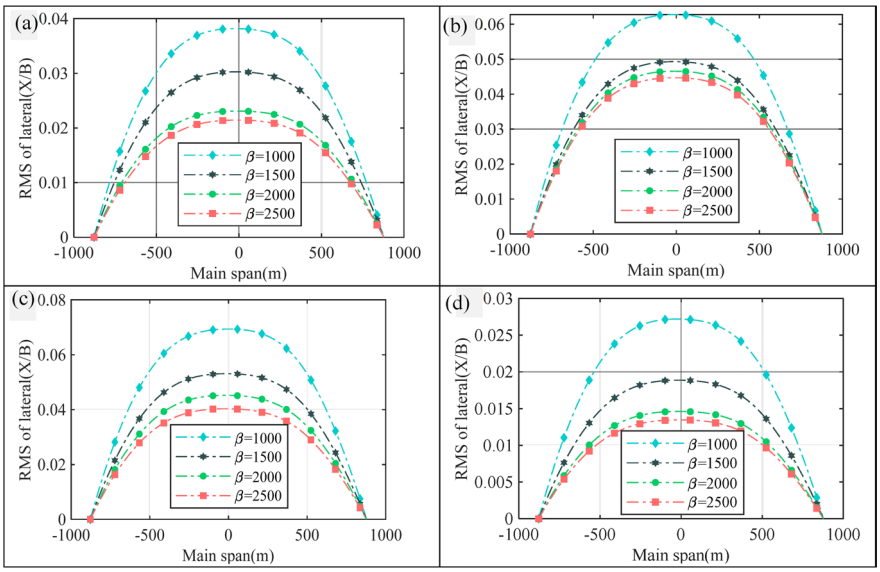

Fig. 9 Lateral displacement comparison of the bridge deck: **a** uMF1; **b** uMF2; **c** NMF1; **d** NMF2

values of torsional displacement under the NMF2 are the smallest. The maximum RMS values of torsional displacement responses under the uMF2 and NMF1 with $\beta = 1000$ are larger than 1°, whereas the maximum RMS values under the uMF1 and NMF2 are only about 0.6° and 0.26°. Furthermore, the RMS values of the vertical displacement under NMF1 are the greatest, and the vertical displacement RMS values of NMF2 are the minimum. Similarly, the RMS values of the lateral displacement at NMF1 are the greatest, while the RMS values of NMF2 are the smallest. Thus, the β in the exponential function has an obvious effect on the displacement responses of the bridge deck, in which the nonlinear buffeting responses under the NMF1 and the NMF2 are the largest and smallest, respectively.

3.3 Buffeting responses under various fluctuating wind velocity models

The time histories of three buffeting displacement responses at the 1/2L mid-span of the bridge deck under the four non-stationary wind velocity models are described in Fig. 10, respectively. There are torsional displacement α, vertical relative displacement Y/H, and lateral relative displacement X/B, where H and B are the height and width of the closed-box girder. The maximum torsional displacement under the NMF2 is the largest and the maximum vertical relative displacement under the uMF1 is the largest among the four models, respectively. In particular, the mean values of torsional displacements under the uMF1, uMF2, NMF1, and NMF2 are 0.0956°, 0.2255°, 0.2283°, and 0.0627°, respectively. The mean square errors of torsional displacements under the uMF1, uMF2, NMF1, and NMF2 are 0.172, 0.311, 0.244, and 0.069, respectively. Furthermore, the mean values of vertical relative displacements under the uMF1, uMF2, NMF1, and NMF2 are -0.1679, -0.1649, -0.1673, and -0.1612, respectively. Their corresponding mean square errors of vertical relative displacements are 0.1849, 0.1809, 0.1757, and 0.179, respectively. Their maximum lateral relative displacement responses are close to 0.068, in which the lateral displacement of uMF1 is the largest. In general, the average square error of torsional

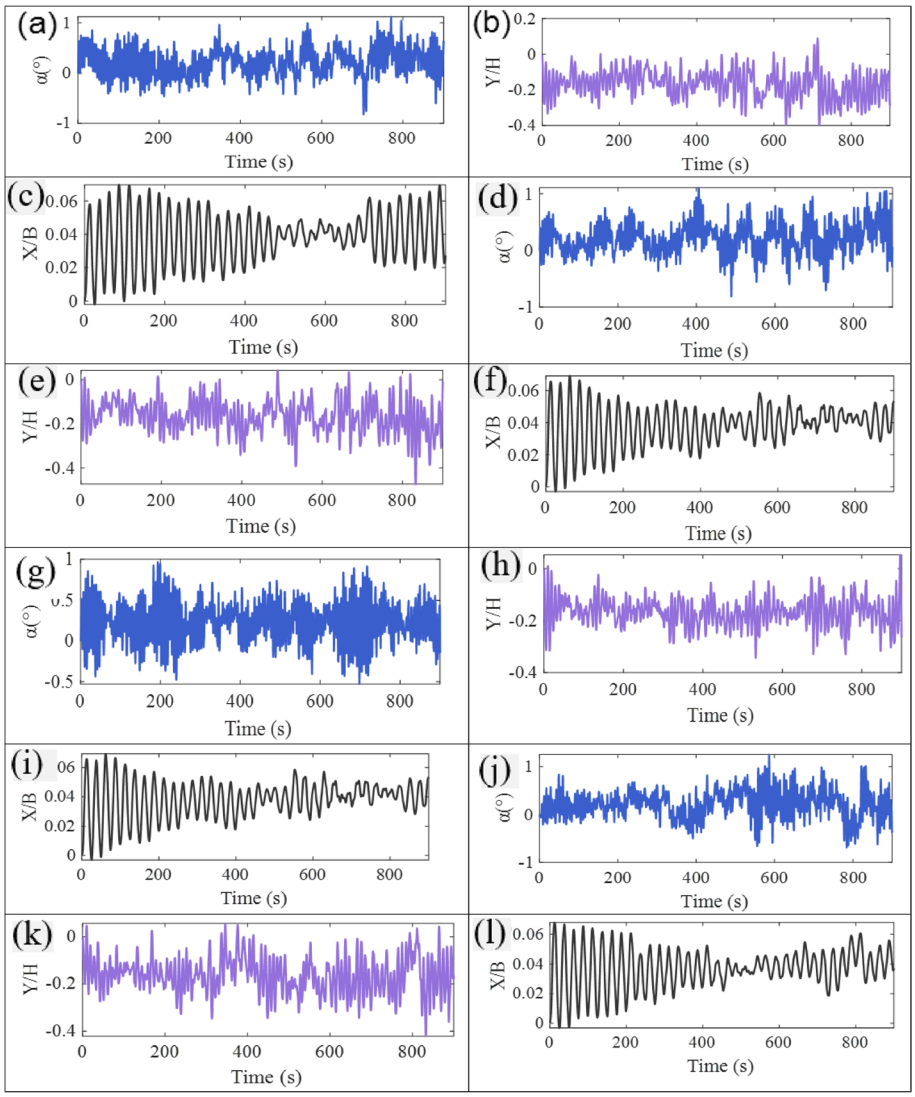

Fig. 10 Time histories of three displacement responses (i.e., torsional, vertical, and lateral) at the mid-span: **a**-**c** uMF1; **d**-**f** uMF2; **g**-**i** NMF1; **j**-**l** NMF2

displacement under the NMF1 is the largest, but the extreme values of vertical and lateral displacements under the uMF1 are the smallest.

Furthermore, three displacement responses along the whole bridge deck under four non-stationary wind velocities and a stationary wind velocity are compared in Fig. 11(a-c), respectively. It shows that the RMS values of the three displacement responses present an obvious symmetrical phenomenon at 1/2L of the main span, and most of the three displacement responses without modulation functions are the smallest. The RMS values of torsional displacement responses under the NMF1 are the largest, while the vertical and lateral displacement responses under the NMF2 are the largest. The three displacement responses at 1/2L under the NMF1 and NMF2 are slightly larger than those under the uMF1and uMF2. Hence, the nonlinear buffeting responses

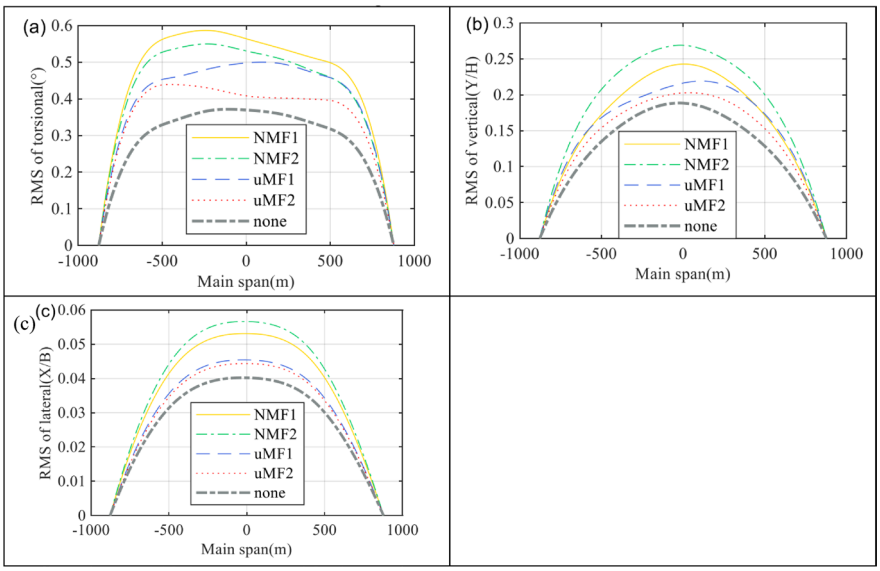

Fig. 11 RMS values comparison of displacement responses of the bridge deck: **a** torsional, **b** vertical, and **c** lateral displacement responses under five wind velocity models

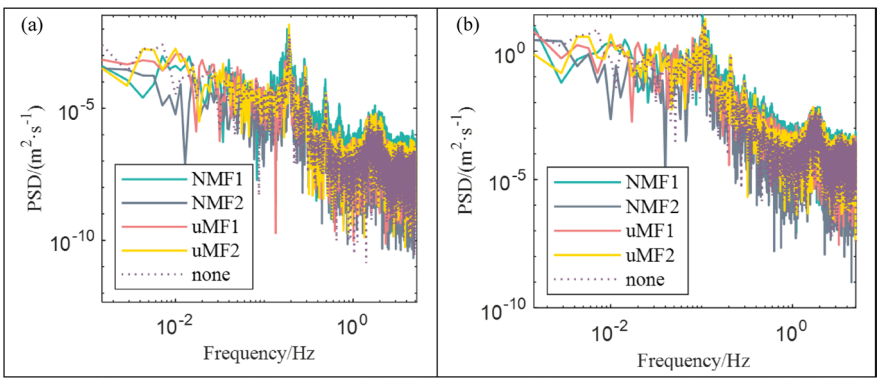

Fig. 12 PSD comparison under five wind velocity models: **a** torsional and **b** vertical displacement responses

of the bridge under non-uniform modulation functions are larger than those with uniform modulation functions.

As shown in Fig. 12, the Power Spectral Density (PSD) for the torsional and vertical displacement responses is given in the case of four non-stationary wind velocities and a stationary wind velocity. Two obvious spectral peaks in the frequency band occur near 0.1 Hz and 1 Hz, and there are some fluctuations of vibrational energy in the time axis for the vertical displacements. The spectral peak values of torsional and vertical displacement responses at high frequencies are smaller than those at a lower frequency, which indicates that most of the vibrational energy is concentrated in the low-frequency range. The values of PSD under the NMF1 are relatively the largest, but the values of PSD under the NMF2 are the relatively smallest. Therefore, the influence of different modulation functions on the energy distribution of nonlinear buffeting responses is very small and the low frequency has a larger peak of PSD.

4 Conclusions

This present study systematically investigated the effect of non-stationary wind velocity models on nonlinear buffeting responses of a super long-span closed-box girder suspension bridge by considering the nonlinear aerodyanmic force effects. The major findings are described as follows:

- Four typical non-stationary wind velocity models are established at the bridge site by combing the average wind velocity of an exponential function and the fluctuating wind velocity of two common modulation functions and non-modulation functions.
- The turbulence intensities using two non-uniform modulation functions are larger than those of two uniform modulation functions, and the four wind velocity models have obvious non-stationary characteristics through the comparison of cross-correlation and power spectrum density.
- With the decrease of the independent variable β in the exponential function of the average wind velocity, the RMS values of three displacement responses along the bridge deck gradually become larger, especially when the β changes from 2000 to 1500.
- Most of the torsional, vertical, and lateral displacement responses along the bridge deck under the uniform modulation function are smaller than those under the non-uniform modulation function, in which the RMS values of the NMF2 and uMF2 are the largest and smallest, respectively.

The buffeting performance of a closed-box girder suspension bridge under non-stationary wind velocity with specific functions was investigated in the paper. The influence of the non-stationary wind of measured strong typhoons on the buffeting performance of suspension bridges will be discussed in further research. The coupling effect of traffic loading and wind loading is very complex due to the randomness [27], which should be studied by the wind-vehicle- bridge system in future.

Acknowledgements
The authors sincerely acknowledge support for this research jointly provided by all the authors and the National Key Laboratory of Green and Long-Life Road Engineering in Extreme Environment.

Authors' contributions
Prof. Rui Zhou carried out the buffeting response analysis and wrote this paper. Dr. Yinan Lin established the four wind velocity models, and provided analysis support. Dr. Peng Lu provided help with the FEM and the writing of this study. Prof. Yongxin Yang gave some advice on the analysis results, and provided funding for this study. Dr. Jinbo Zhu gave some advice during the revision of this manuscript. All authors read and approved the final manuscript.

Funding
The funding of this research work was jointly provided by the National Natural Science Foundation of China (Nos. 52278311, 52178503, U2005216, and 51908374), the Guangdong Basic and Applied Basic Research Foundation (No. 2023A1515030148), the Shenzhen Science and Technology Innovation Program (Nos. JCYJ20220531101609020, KQTD20200820113004005, and GJHZ20220913143006012), the Foundation of State Key Laboratory for Disaster Reduction in Civil Engineering, Tongji University (No. SLDRCE19-B-10), and the National Key Laboratory of Green and Long-Life Road Engineering in Extreme Environment.

Availability of data and materials
The data and materials used to support the findings of this study are available from the corresponding author upon request.

Declarations

Competing interests
The authors declare no potential conflicts of interest concerning the research, authorship, and/or publications of this article.

Received: 2 July 2023 Accepted: 19 September 2023
Published online: 17 October 2023

References

1. Zhou R, Ge YJ, Yang YX et al (2018) Wind-induced nonlinear behaviors of twin-box girder bridges with various aerodynamic shapes. Nonlinear Dyn 94:1095–1115. https://doi.org/10.1007/s11071-018-4411-y
2. Lei SM, Cui W, Patruno L et al (2022) Improved state augmentation method for buffeting analysis of structures subjected to non-stationary wind. Probabilist Eng Mech 69:103309. https://doi.org/10.1016/j.probengmech.2022.103309
3. Zhou R, Lu P, Gao XD et al (2023) Role of moveable guide vane with various configurations in controlling the vortex-induced vibration of twin-box girder suspension bridges: An experimental investigation. Eng Struct 281:115762. https://doi.org/10.1016/j.engstruct.2023.115762
4. Su Y, Huang GQ, Liu R et al (2021) Efficient buffeting analysis under non-stationary winds and application to a mountain bridge. Wind Structs 32(2):89–104. https://doi.org/10.12989/was.2021.32.2.89
5. Qin Z, Xia D, Dai L et al (2022) Investigations on wind characteristics for typhoon and monsoon wind velocitys based on both stationary and non-stationary models. Atmosphere 13(2):178. https://doi.org/10.3390/atmos13020178
6. Wang H, Xu ZD, Yang M et al (2021) Numerical analysis on buffeting performance of a long-span four-tower suspension bridge using the FEM model. KSCE J Civ Eng 25:854–865. https://doi.org/10.1007/s12205-021-2406-6
7. Zhou R, Ge YJ, Liu SY et al (2020) Nonlinear flutter control of a long-span closed-box girder bridge with vertical stabilizers subjected to various turbulence flows. Thin Wall Struct 149:106245. https://doi.org/10.1016/j.tws.2019.106245
8. Xu YL, Chen J (2004) Characterizing nonstationary wind speed using empirical mode decomposition. J Struct Eng 130(6):912–920. https://doi.org/10.1061/(ASCE)0733-9445(2004)130:6(912)
9. Hu L, Xu YL (2014) Extreme value of typhoon-induced non-stationary buffeting response of long-span bridges. Probabilist Eng Mech 36:19–27. https://doi.org/10.1016/j.probengmech.2014.02.002
10. Zhao L, Cui W, Ge YJ (2019) Measurement, modeling and simulation of wind turbulence in typhoon outer region. J Wind Eng Ind Aerodyn 195:104021. https://doi.org/10.1016/j.jweia.2019.104021
11. Han WS, Liu HJ, Wu J et al (2017) Numerical simulation of three-dimensional hurricane wind field around a long-span bridge. J Vib Shock 36(24):77–84 (in Chinese)
12. He XH, Qin HX, Tao TY et al (2017) Measurement of non-stationary characteristics of a landfall typhoon at the Jiangyin Bridge site. Sensors 17(10):2186. https://doi.org/10.3390/s17102186
13. Bao X, Li C (2019) Fast simulation of non-stationary wind velocity based on time-frequency interpolation. J Wind Eng Ind Aerodyn 193:103982. https://doi.org/10.1016/j.jweia.2019.103982
14. Tubino F, Solari G (2020) Time varying mean extraction for stationary and non-stationary winds. J Wind Eng Ind Aerodyn 203:104187. https://doi.org/10.1016/j.jweia.2020.104187
15. Kareem A, Wu T (2013) Wind-induced effects on bluff bodies in turbulent flows: Nonstationary, non-Gaussian and nonlinear features. J Wind Eng Ind Aerodyn 122:21–37. https://doi.org/10.1016/j.jweia.2013.06.002
16. Hu L, Xu YL, Huang WF (2013) Typhoon-induced non-stationary buffeting response of long-span bridges in complex terrain. Eng Struct 57:406–415. https://doi.org/10.1016/j.engstruct.2013.09.044
17. Li YL, Togbenou K, Xiang HY et al (2017) Simulation of non-stationary wind velocity field on bridges based on Taylor series. J Wind Eng Ind Aerodyn 169:117–127. https://doi.org/10.1016/j.jweia.2017.07.005
18. Tao TY, Wang H, Li H (2020) Stationary and non-stationary buffeting analyses of a long-span bridge under typhoon winds. Wind Structs 31(5):445–457. https://doi.org/10.12989/was.2020.31.5.445
19. Tao TY, Xu YL, Huang ZF et al (2020) Buffeting analysis of long-span bridges under typhoon winds with time-varying spectra and coherences. J Struct Eng 146(12):04020255. https://doi.org/10.1061/(ASCE)ST.1943-541X.0002835
20. Huang ZF, Xu YL, Zhan S (2021) Conditionally simulating nonstationary typhoon winds with time-varying coherences for long-span bridges. J Wind Eng Ind Aerodyn 212:104599. https://doi.org/10.1016/j.jweia.2021.104599
21. Yang YX, Ge YJ, Zhou R et al (2020) Aerodynamic countermeasure schemes of super long-span suspension bridges with various aspect ratios. Int J Struct Stab Dyn 20(5):2050061. https://doi.org/10.1142/S0219455420500613
22. Li JH, Li CX, Shen JH (2009) Numerical simulation of non-stationary fluctuating wind velocity. J Vib Shock 28(1):18–23 (In Chinese)
23. Tao TY, Wang H, Wu T (2016) Comparative study of the wind characteristics of a strong wind event based on stationary and nonstationary models. J Struct Eng 143(5):04016230. https://doi.org/10.1061/(ASCE)ST.1943-541X.0001725
24. Zhou R, Ge YJ, Liu QK et al (2021) Experimental and numerical studies of wind-resistance performance of twin-box girder bridges with various grid plates. Thin Wall Struct 166:108088. https://doi.org/10.1016/j.tws.2021.108088
25. Li M, Li MS, Sun YG (2021) Effects of turbulence integral scale on the buffeting response of a long-span suspension bridge. J Sound Vib 490:115721. https://doi.org/10.1016/j.jsv.2020.115721
26. Zhou R, Yang YX, Ge YJ et al (2015) Practical countermeasures for the aerodynamic performance of long span cable-stayed bridge with open decks. Wind Structs 21(2):223–239. https://doi.org/10.12989/was.2015.21.2.223
27. Maizuar M, Zhang LH, Miramini S et al (2017) Detecting structural damage to bridge girders using radar interferometry and computational modelling. Struct Control Health Monit 24(10):e1985. https://doi.org/10.1002/stc.1985

Publisher's Note